



Research article

The staging of nonalcoholic fatty liver disease fibrosis: A comparative study of MR elastography and the quantitative DCE-MRI exchange model

Hao Ren^a, Dawei Yang^a, Hui Xu^a, Xiaofei Tong^b, Xinyan Zhao^b, Qianyi Wang^b, Yameng Sun^b, Xiaojuan Ou^b, Jidong Jia^b, Hong You^b, Zhenchang Wang^a, Zhenghan Yang^{a,*}

^a Department of Radiology, Beijing Friendship Hospital, Capital Medical University, Yongan Road 95, West District, Beijing, 100050, China

^b Liver Research Center, Beijing Friendship Hospital, Capital Medical University, No. 95 Yongan Road, West District, Beijing, 100050, China

ARTICLE INFO

Keywords:

NAFLD
Liver fibrosis
MRE
DCE-MRI

ABSTRACT

Objectives: To evaluate the efficacy and image processing time of the dynamic contrast-enhanced MRI (DCE-MRI) exchange model in liver fibrosis staging and compare it to the efficacy of magnetic resonance elastography (MRE).

Methods: The subjects were 45 patients with nonalcoholic fatty liver disease (NAFLD) who underwent MRE and DCE-MRI in our hospital. Liver biopsy results were available for all patients. Spearman rank correlation coefficients were used to compare the correlations among MRE, DCE-MRI and liver fibrosis parameters. Quantitative DCE-MRI parameters, MRE-derived liver stiffness measurement (LSM), and the results of a combined DCE-MRI + MRE logistic regression model were compared in terms of the area under the receiver operating characteristic curve (AUC). We also compared the scanning and postprocessing times of the MRE and DCE-MRI techniques.

Results: The correlation coefficients between the following parameters of interest and liver fibrosis were as follows: capillary permeability–surface area product (PS; DCE-MRI parameter), -0.761 ; portal blood flow (Fp; DCE-MRI parameter), -0.754 ; MRE-LSM, 0.835 . Some DCE-MRI parameters (PS, Fp) had slightly greater AUC values than MRE-LSM for diagnosing the presence or absence of liver fibrosis, and the combined model had the highest AUC value for all stages except F4, but there was no significant difference in the diagnostic efficacy of the DCE-MRI, MRE, and combined models for any stage of fibrosis. The average scanning times for MRE and DCE-MRI were 17 s and 330 s, respectively, and the average postprocessing times were 45.5 s and 342.7 s, respectively.

Conclusions: In the absence of MRE equipment, DCE-MRI represents an alternative technique. However, MRE is a quicker and simpler method for assessing fibrosis than DCE-MRI in the clinic.

1. Introduction

Nonalcoholic fatty liver disease (NAFLD) is the most common chronic liver disease in the world, and its prevalence can be as high as

* Corresponding author.

E-mail address: yangzhenghan@vip.163.com (Z. Yang).

<https://doi.org/10.1016/j.heliyon.2024.e24558>

Received 16 October 2023; Received in revised form 18 December 2023; Accepted 10 January 2024

Available online 18 January 2024

2405-8440/© 2024 Published by Elsevier Ltd.

This is an open access article under the CC BY-NC-ND license

(<http://creativecommons.org/licenses/by-nc-nd/4.0/>).

Abbreviations

ECM =	Extracellular matrix
EES =	Extravascular extracellular space
HSCs =	Hepatic stellate cells
HPI =	Hepatic perfusion coefficient
MRE =	MR elastography
DCE-MRI =	dynamic contrast-enhanced MRI
NAFLD =	Nonalcoholic fatty liver disease
FP =	Plasma blood flow
PS =	Permeability of capillary vessel surface
2CXM =	Two-compartment exchange model

30 % in adults [1,2]. In the past 40 years, exclusive diagnostic criteria have been adopted for NAFLD. With the improvement of the basic level of pathophysiology, people's understanding of NAFLD has also been constantly changing. Experts believe that affirmative diagnostic criteria should be adopted for NAFLD. In 2020, NAFLD welcomed its first renaming, Asian Pacific Association for the Study of the Liver (APASL) suggestions for the use of metabolic-dysfunction-associated fatty liver disease (MAFLD) in NAFLD [3]. During the 2023 European Association for the Study of the Liver (EASL) Annual Conference, the "A multisociety Delphi consensus statement on new fatty liver disease nomenclature" was officially released [4]. The new consensus suggests renaming NAFLD as "metabolic dysfunction-associated steatotic liver disease (MASLD), which places more emphasis on the role of metabolic cardiovascular risk factors in the pathogenesis of NAFLD. Renaming NAFLD is a broad and complex task, and the results of the latest renaming are still uncertain [5]. Due to incomplete uniformity of names, various studies on NAFLD, MAFLD, and MASLD exist. The main pathological manifestations of NAFLD are steatosis, inflammation, and fibrosis; steatosis and the inflammatory component of the NAFLD activity score (NAS) do not correlate with overall disease-specific mortality. The risk of liver-related death increases exponentially as the fibrosis stage progresses [6–8]. Early fibrosis in NAFLD is typically reversible, so early detection of liver fibrosis is clinically significant [9,10]. Risk stratification is also performed to manage advanced fibrosis in NAFLD patients [11]. In clinical practice, the invasive technique of liver aspiration biopsy is commonly used to diagnose liver fibrosis; because the biopsy is only a local sample, there is a potential risk of sampling error, which limits the clinical application of this technique in patient follow-up [9,12]. Therefore, there is a need to develop a noninvasive method of assessing liver fibrosis in NAFLD patients in the clinic.

With new technologies such as magnetic resonance elastography (MRE) and dynamic contrast-enhanced MRI (DCE-MRI), quantitative assessment of liver fibrosis staging can be accomplished by radiology. MRE is based on displacement phase imaging technology, which utilizes different wavelengths of mechanical wave conduction in different elastic media and particle displacement of tissue under the action of shear waves and calculates a quantitative elastogram of liver tissue with an inversion algorithm; accordingly, the MRE technique can be performed to determine the degree of liver fibrosis intuitively, thus effectively distinguishing the different stages of fibrosis. In previous studies, MRE was found to have high diagnostic efficacy for liver fibrosis [13–15]. However, MRE requires special hardware whose clinical availability is limited. In addition, MRE scans will fail in patients with iron overload or obesity [16].

DCE-MRI does not have the above limitations described for MRE applications. DCE-MRI allows semiquantitative and quantitative analysis of the hemodynamic status of tissue perfusion and microvascular permeability [17,18]. The progression of liver fibrosis is often accompanied by changes in the hemodynamic and microvascular environments, and hemodynamic changes precede morphological changes [19]. Therefore, tissue perfusion and microvascular permeability were calculated by DCE-MRI to reflect the hemodynamic changes in the liver and thus assess liver fibrosis.

At present, the Tofts model is the most widely used pharmacokinetic model of DCE-MRI hemodynamics [20,21]. The latest model is the two-compartment exchange model (2CXM); however, in contrast to the Tofts model, the 2CXM separates the perfusion influences from K_{trans} and thus obtains the true capillary permeability–surface area product (PS) parameter so that changes in hepatic microcirculatory perfusion can be assessed more accurately in theory [22].

Quantitative DCE-MRI is commonly used in animal experiments [23–25], while clinical studies mainly use semiquantitative DCE-MRI parameters [26–28]. In a study by S. Kelle et al. [23], semiquantitative DCE-MRI was found to have lower diagnostic efficacy for liver fibrosis than DWI. In animal experiments by Zou L [26], full quantitative DCE-MRI showed the opposite result. In a study by Li et al. [29], the K_{trans} parameter of the Tofts model for DCE-MRI was found to have an AUC diagnostic validity of 0.887 in an early fibrosis diagnosis.

Quantitative DCE-MRI has demonstrated higher diagnostic efficacy than semiquantitative DCE-MRI in previous studies, and the diagnostic accuracy of quantitative DCE-MRI in the noninvasive assessment of liver fibrosis merits investigation.

According to previous studies, DCE-MRI may represent an alternative to MRE; thus, the purpose of this study was to explore the diagnostic efficacy of the quantitative DCE-MRI exchange model for each liver fibrosis stage and to compare the diagnostic ability of DCE-MRI and MRE for different stages of liver fibrosis. The development of noninvasive fibrosis assessment techniques also involves consideration of their ease of clinical application; thus, scanning and postprocessing times need to be considered. Therefore, this study also compared the scanning and postprocessing times of the MRE and DCE-MRI techniques.

2. Materials and methods

2.1. Experimental design and inclusion and exclusion criteria

This study was a single-center retrospective study. The Ethics Committee of Beijing Friendship Hospital approved this study (2020-P2-235-01) and waived informed consent given its retrospective design. This study was conducted on patients with pathologically diagnosed NAFLD who underwent DCE-MRI and MRE (73 individuals between November 2016 and September 2021). The exclusion criteria for patients were as follows: (1) MRE or DCE-MRI data that did not meet the image quality requirements (7 patients were excluded), (2) focal liver lesions ≥ 3 cm on MRI (1 patient was excluded), or (3) F0–F3 liver puncture pathology and an imaging interval > 6 months (20 patients were excluded). The total number of exclusions was 28. The flow chart of subject inclusion and exclusion is shown in Fig. 1.

2.2. Reference standards

All patients underwent ultrasound-guided liver biopsy, and one strip of liver tissue (more than 15 mm in length and containing at least six confluent areas) was collected from the right liver lobe in each patient. The total number of patients excluded was 28. The flow chart of subject inclusion and exclusion is shown in Fig. 1. All pathological tissue samples were stained with hematoxylin-eosin stain and Masson trichrome stain. All pathological findings were pathologically diagnosed by a senior hepatologist (XYZ) with more than ten years of experience who was aware of each patient's clinical profile but had no knowledge of the subject's imaging measurements. The Nonalcoholic Steatohepatitis Clinical Research Network histologic scoring system for fibrosis was used. Fibrosis was staged as follows: F0: no fibrosis; F1: perisinusoidal or periportal fibrosis; F2: perisinusoidal and portal/periportal fibrosis; F3: bridging fibrosis; and F4: cirrhosis.

2.3. Image acquisition and postprocessing

All subjects were scanned on a 3.0 T MRI instrument (GE Discovery 750 W) with scan sequences including MRE and DCE-MRI, and MRI signals were acquired using a 16-channel phased-array coil.

2.4. DCE-MRI scan parameters and postprocessing

The DCE-MRI scan parameters were as follows: repetition time/echo time (T_R/T_E), 3.2 ms/1.4 ms; matrix, 256×160 , field of view (FOV), $42 \text{ cm} \times 35.7 \text{ cm}$; layer thickness, 4 mm; layer spacing, 0 mm; flip angle, 12° ; and receiver bandwidth, $\pm 83.33 \text{ kHz}$. The liver acquisition with volume acceleration–extended volume (LAVA-XV) sequence was used to cover the whole liver, and the radiologic technologist scanned the mask image before enhancement, followed by breath-hold training to keep the subject performing intermittent and low-frequency breathing. The contrast agent was then injected intravenously into the upper arm, and images were acquired continuously by scanning 30 phases with a temporal resolution of 10 s for a total of 5 min. The injection method was as follows: a high-pressure MRI injector (Medrad Spectris Solaris EP) was used to inject the contrast agent GD-DTPA (at a dose of 0.1 mmol/kg) first, followed by 20 mL of saline, all at a rate of 2.5 mL/s. The DCE-MRI sequence took 5 min and 30 s.

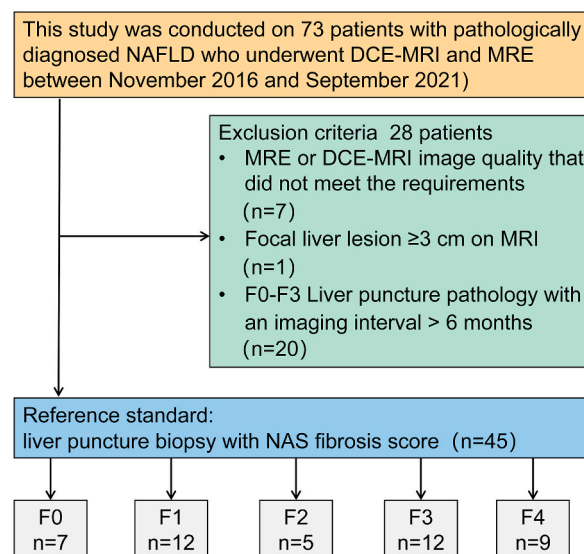


Fig. 1. Flowchart of inclusion and exclusion criteria.

The 2CXM is the most commonly used exchange model and is capable of measuring portal blood flow (Fp) and PS separately, as well as Ve, Vp, and Kep data [30,31]. The calculation formula of Exchange is shown in Equation (1).

$$Ct(t) = Fp[faCa(t) + (1 - fa)Cv(t)] / (1 - HLV) \otimes A.exp(-\alpha t) + (1 - A).exp(-\beta) \tag{1}$$

A, α , and β were obtained according to the hemodynamic model parameters Vp, Ve, and PS. The relationship between Ktrans and the values of Fp and PS is shown in Equation (2).

$$Ktrans = Fp(1 - e^{-PS/Fp}) \tag{2}$$

The parameters of Equations (1) and (2) are shown in Table 1, and a schematic diagram of the exchange is shown in Fig. 2.

The radiologist imported the scanned images into GE's Omni Kinetics software for processing. A dual-input AIF model was selected, with the abdominal aorta and portal vein labeled as the vascular input function. The fitted curves used to select the exchange model for calculation are shown in Fig. 3. Two radiologists, HR (with eight years of experience) and DWY (with more than 10 years of experience), who were unaware of the pathological findings, selected three ROIs in the right lobe and segment 4 on the largest slice of the liver and calculated the mean. The ROIs were selected, avoiding the hepatic margins, blood vessels and hepatic cyst areas. The final values were averaged from the measurements performed by the two radiologists, and the ROIs are shown in Fig. 3. Two radiologists recorded the postprocessing time for each patient.

2.5. MRE image acquisition and processing

The MRE scan parameters were as follows: spin-echo echo-planar imaging (SE-EPI); TR/TE: 1000 ms/min full; matrix: 64 × 64; FOV: 42 cm × 42 cm; layer thickness: 10 mm; layer spacing: 5 mm; number of layers, 7; number of excitations, 1; bandwidth: ±250 kHz; driver frequency, 60 Hz; amplitude, 70 %; end-expiratory breath-hold scan; and a scanning duration of 17 s.

All acquired MRE images were automatically processed by the postprocessing software Volume Viewer (version 13.0, GE Healthcare) on the MR master computer, and wave images, elastograms, and magnitude images were generated using inversion algorithms. The elastogram forms crossed line regions (low-confidence data regions excluded by the postprocessing algorithm).

Two radiologists (the same two as before) selected the ROI (right branch level of the portal vein) in the right lobe region of the liver, including the two layers above this level and a total of three layers, using a weighted average for the measurements. The physicians drew the ROI to include as much of the liver parenchyma as possible, with a minimum area >3 cm², while avoiding large vessels, bile ducts, and areas in the 1 cm surrounding the liver or in the cross-shadow areas (low-confidence data areas). Two radiologists recorded the postprocessing time for each patient.

2.6. Statistical analysis

In this study, PASS software 15.0 was used to calculate the necessary sample size. Given α err pro = 0.05, Power (1- β err pro) = 0.80, the estimated AUC of DCE-MRI was 0.8, compared with AUC 0.5, N+ = 13 calculated from N- = 7; accordingly, the initial calculation required 20 cases, and to ensure the credibility of this study, this study collected a total of 45 cases.

All data were statistically analyzed using SPSS 25.0 software and MedCalc 19.0. The Shapiro–Wilk test was used to test the normality of the data. Data for all measurements were expressed as the mean ± standard deviation (normally distributed data) or median and quartiles (nonnormally distributed). The Kruskal-Wallis test was used to compare the differences in fibrosis stages among different groups of different parameters. A Spearman's rank correlation coefficient $\rho > 0.8$ was considered very strong, a ρ of 0.6–0.8 was moderately strong, a ρ of 0.3–0.6 was fair, and a $\rho < 0.3$ was poor [32]. A combined DCE-MRI model was constructed to include the strongly correlated parameters that were substituted into the linear regression equation and tested for covariance. DCE-MRI-related parameters and MRE were used to construct the logistic regression model. The diagnostic efficacy of each MR parameter and combined model were then tested using the receiver operating characteristic (ROC) curve. Cutoff values, sensitivity, and specificity were

Table 1
Exchange formula symbols and abbreviations and definitions.

Symbol/Abbreviation	Definition	Unit
Ct(t)	Contrast agent concentration in tissue	mmol/L
Ca(t)	Abdominal aortic contrast agent concentration	mmol/L
Cp(t)	Portal vein contrast agent concentration	mmol/L
fa	Intratissue arterial perfusion fraction	%
HLV	Intravascular hematocrit	None
HPI	Hepatic perfusion coefficient	None
Fp	Plasma blood flow	ml/ml·min ⁻¹
Vp	Blood plasma volume fraction	None
Ve	Extravascular extracellular space volume fraction	None
Kep	Outflow rate constant	min ⁻¹
Ktrans	Inflow transfer constant	min ⁻¹
PS	Permeability of the capillary vessel surface	ml/ml·min ⁻¹
⊗	Convolution operation	None

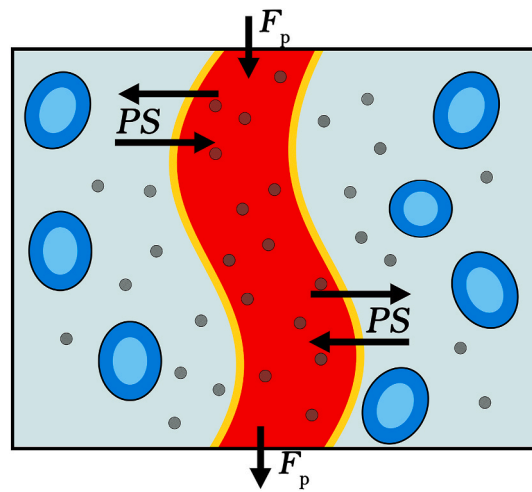


Fig. 2. Schematic of the dynamic exchange model. PS indicates the capillary permeability–surface area product. F_p indicates portal blood flow.

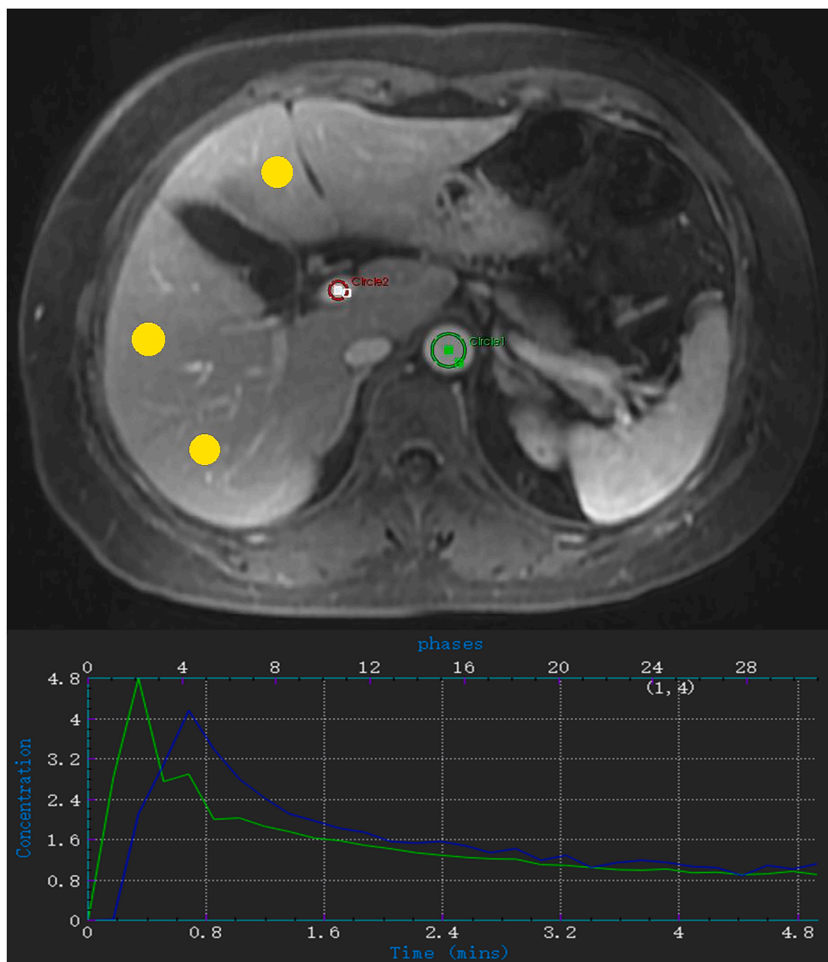


Fig. 3. Abdominal aorta (green circles) and portal vein input (red circles) labeling and the 3 ROI labeling areas (yellow circular areas) for each DCE-MRI parameter. The curved part of the picture shows the fitted curve measurements of the abdominal aorta (green line) and portal vein (blue line). (For interpretation of the references to colour in this figure legend, the reader is referred to the Web version of this article.)

determined by calculating the maximum Youden index. In the dichotomous grouping, the fibrosis group ($F \geq 1$), significant fibrosis group ($F \geq 2$), advancing fibrosis group ($F \geq 3$), and cirrhosis group ($F = 4$) were defined as positive results, and the DeLong test was used to compare the area under the ROC curve (AUC) values of the multiparametric combined diagnostic model and the single-parameter models.

3. Results

3.1. Subject information

Ultimately, 45 subjects were included, all of whom had NAFLD; the subjects comprised 15 males and 30 females, with a mean age of 50 ± 12 years and a mean body mass index (BMI) of 26.673 ± 3.001 . There were 7 patients in stage F0, 12 patients in stage F1, five patients in stage F2, 12 patients in stage F3, and nine patients in stage F4. Sample plots of patients in stages F0 and F3 are shown in Figs. 4 and 5, respectively.

3.2. Correlation between the value of each quantitative parameter and the stage of liver fibrosis

MRE, PS, Fp, and HPI were strongly correlated with liver fibrosis ($\rho = 0.835, -0.761, -0.754$, and 0.632 , respectively; all $P < 0.001$); Vp had a fair correlation with liver fibrosis ($\rho = -0.361, P < 0.05$); Ve and Kep were not correlated with liver fibrosis (all $P > 0.05$). The correlation of each parameter with fibrosis is shown in Table 2. MRE had the highest correlation with the stage of liver fibrosis as determined by pathology. The DCE-MRI (PS, Kep, Ve, Vp, HPI, Fp) parameters and MRE-LSM used the Kruskal-Wallis test to compare the differences in fibrosis stages among various parameters. There was a statistically significant difference in the values of different fibrosis groups between DCE-MRI (PS, Vp, HPI, Fp) and MRE ($P < 0.05$), as shown in Fig. 4(A–F) and 5 (A–F). There was no difference in the values of Kep and Ve in the different fibrosis groups ($P > 0.05$). Values of DCE-MRI and MRE quantitative parameters in different liver fibrosis stages are shown in Table 3.

3.3. Comparison of the diagnostic efficacy of DCE-MRI parameters alone and in combination with MRE elasticity values

A combined DCE-MRI model was constructed to include the strongly correlated parameters (PS, Fp, and HPI), which were substituted into the linear regression equation and tested for covariance. The variance inflation factors of PS and Fp were 20.254 and 20.155, respectively; therefore, the PS parameters with high correlation coefficients were selected to be included in the combined diagnostic model by logistic regression to construct a combined DCE-MRI model, i.e., combined model 1 (PS, HPI), and a combined DCE-MRI and MRE model 2 (PS, HPI, and MRE-LSM).

The sensitivity and specificity of all AUCs, optimal cutoff values, and different diagnostic models for detecting any fibrosis (F0 versus F1–4), significant fibrosis (F0–1 versus F2–4), advanced fibrosis (F0–2 versus F3–4), and cirrhosis (F0–3 versus F4) are shown in Table 4 and Fig. 6(A–D). The AUC values of DCE-MRI were higher than the MRE-LSM in the diagnosis of early fibrosis. There was no significant difference in the AUC of DCE-MRI (PS, HPI), MRE-LSM, and combined models 1 and 2 in the diagnosis of different stages of fibrosis ($P > 0.05$).

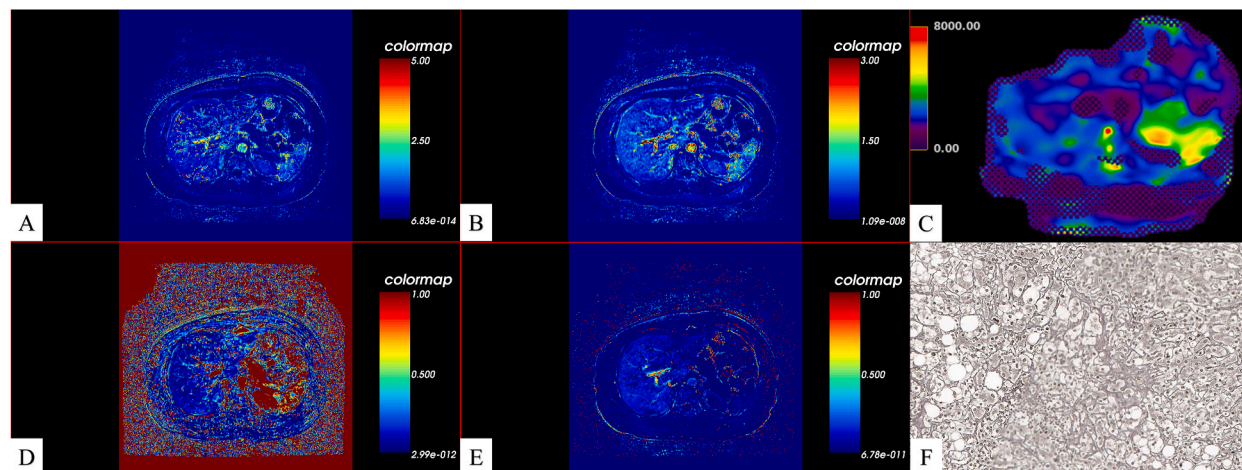


Fig. 4. A 40-year-old female patient was pathologically confirmed to be in stage F0 by needle biopsy. From A to F, the images show PS, Fp, MRE, HPI, Vp, and Masson staining, with values of $0.606 \text{ mL/mL}\cdot\text{min}^{-1}$, $0.558 \text{ mL/mL}\cdot\text{min}^{-1}$, 2.122 kPa , 0.127 , and 0.130 , respectively, for the first 5 images.

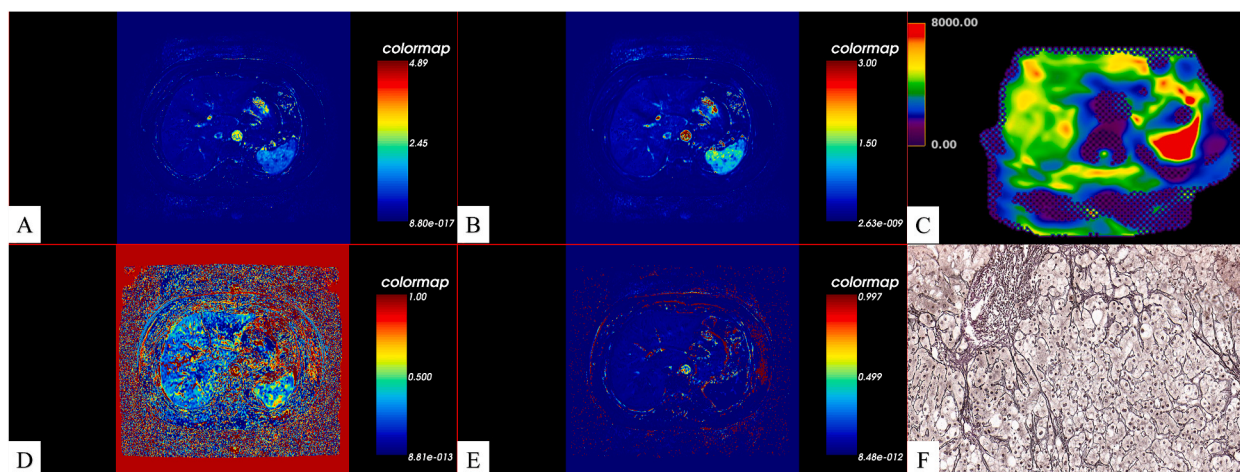


Fig. 5. A 59-year-old female patient was pathologically confirmed to be in stage F3 by needle biopsy. From A to F, the images show PS, Fp, MRE, HPI, Vp, and Masson staining, with values of 0.276 mL/mL-min⁻¹, 0.0251 mL/mL-min⁻¹, 4.178 kPa, 0.371, and 0.037, respectively, for the first 5 images.

Table 2
Correlation of each parameter with liver fibrosis.

Parameter	ρ	P
PS	-0.761	< 0.001 ^a
Fp	-0.754	< 0.001 ^a
Kep	-0.215	0.156
Ve	0.017	0.913
Vp	-0.361	0.015 ^a
HPI	0.632	< 0.001 ^a
MRE	0.835	< 0.001 ^a

^a Indicates statistical significance.

Table 3
Values of DCE-MRI and MRE quantitative parameters in different liver fibrosis stages.

Group	F0 (n = 7)	F1 (n = 12)	F2 (n = 5)	F3 (n = 12)	F4 (n = 9)	P
PS (ml/ml-min ⁻¹)	0.649 (0.586, 0.702)	0.532 (0.471, 0.633)	0.487 (0.350, 0.507)	0.291 (0.262, 0.411)	0.314 (0.216, 0.382)	< 0.001 ^a
Fp (ml/ml-min ⁻¹)	0.607 (0.449, 0.701)	0.471 (0.441, 0.580)	0.443 (0.308, 0.473)	0.264 (0.227, 0.326)	0.307 (0.199, 0.336)	< 0.001 ^a
Kep (min ⁻¹)	4.944 (2.984, 5.512)	3.437 (1.167, 6.220)	2.684 (1.706, 3.584)	2.442 (0.737, 4.300)	4.200 (0.842, 5.549)	0.300
Ve	0.179 (0.145, 0.340)	0.407 (0.158, 0.777)	0.504 (0.342, 0.611)	0.472 (0.224, 0.697)	0.141 (0.077, 0.586)	0.206
Vp	0.104 (0.083, 0.134)	0.091 (0.074, 0.143)	0.067 (0.052, 0.153)	0.053 (0.039, 0.092)	0.069 (0.041, 0.114)	0.039 ^a
HPI	0.171 (0.049, 0.242)	0.149 (0.082, 0.260)	0.291 (0.222, 0.442)	0.409 (0.333, 0.492)	0.535 (0.332, 0.727)	0.001 ^a
MRE (kPa)	2.284 (2.171, 2.590)	2.538 (2.180, 2.745)	2.617 (2.395, 3.306)	4.352 (3.207, 5.504)	6.894 (4.523, 7.953)	< 0.001 ^a

^a Indicates statistical significance.

3.4. The scanning and postprocessing times of the MRE and DCE-MRI techniques

The average MRE scanning time was 17 s, and the average postprocessing time was 45.5 s, for a total of 62.5 s. The average DCE-MRI scanning time was 330 s, and the average postprocessing time was 342.7 s, for a total of 672.7 s. Paired-sample t tests were performed to compare the postprocessing time and total time of the DCE-MRI and MRE techniques; $P < 0.001$ was considered to indicate a statistically significant difference.

4. Discussion

In this study, the parameter most strongly correlated with the pathological stage of liver fibrosis was MRE-LSM ($\rho = 0.835$), which had a stronger correlation than any of the DCE-MRI parameters. The AUCs of the single DCE-MRI parameter (PS) and the combined

Table 4
Diagnostic efficacy of PS, HPI, MRE, combined model 1, and combined model 2 for liver fibrosis.

Parameter	Cut-off	Sensitivity (%)	Specificity (%)	PPV (%)	NPV (%)	Z	P	AUC (95 % CI)
F0 vs. F1-4								
PS (ml/ml·min ⁻¹)	≤0.551	86.84	85.71	97.06	54.55	7.221	<0.001	0.906 (0.781–0.973)
HPI	>0.252	65.79	100.00	100.00	35.01	4.220	<0.001	0.805 (0.659–0.907)
MRE (kPa)	>2.682	65.79	100.00	100.00	35.01	5.274	<0.001	0.838 (0.698–0.931)
Combined model 1	>0.721	86.84	85.71	97.06	54.55	7.695	<0.001	0.910 (0.786–0.975)
Combined model 2	>0.634	89.47	85.71	97.14	60.00	8.008	<0.001	0.917 (0.796–0.978)
F0-1 vs. F2-4								
PS (ml/ml·min ⁻¹)	≤0.460	84.62	89.47	91.67	80.95	10.861	<0.001	0.923 (0.804–0.981)
HPI	>0.261	80.77	89.47	91.30	77.27	5.408	<0.001	0.844 (0.705–0.935)
MRE (kPa)	>2.921	84.62	100.00	100.00	82.61	12.499	<0.001	0.937 (0.823–0.988)
Combined model 1	>0.599	80.77	89.47	91.30	77.27	10.704	<0.001	0.921 (0.801–0.980)
Combined model 2	>0.725	80.77	100.00	100.00	79.17	20.733	<0.001	0.964 (0.860–0.997)
F0-2 vs. F3-4								
PS (ml/ml·min ⁻¹)	≤0.437	95.24	87.50	86.96	95.46	9.273	<0.001	0.917 (0.795–0.978)
HPI	>0.291	85.71	83.33	81.82	86.95	5.006	<0.001	0.829 (0.688–0.925)
MRE (kPa)	>3.090	95.24	95.83	95.24	95.83	21.920	<0.001	0.972 (0.874–0.999)
Combined model 1	>0.330	95.24	87.50	86.96	95.46	9.580	<0.001	0.919 (0.798–0.979)
Combined model 2	>0.540	95.24	100.00	100.00	96.00	26.072	<0.001	0.982 (0.889–1.000)
F0-3 vs. F4								
PS (ml/ml·min ⁻¹)	≤0.394	100.00	66.67	42.86	100.00	4.656	<0.001	0.806 (0.660–0.908)
HPI	>0.488	66.67	88.89	60.00	91.43	3.800	<0.001	0.809 (0.664–0.910)
MRE (kPa)	>4.184	88.89	83.33	57.14	96.77	10.154	<0.001	0.929 (0.811–0.984)
Combined model 1	>0.337	66.67	91.67	66.68	91.67	5.206	<0.001	0.843 (0.703–0.934)
Combined model 2	>0.057	100.00	75.00	50.00	100.00	10.248	<0.001	0.926 (0.807–0.983)

PPV, positive predictive value; NPV, negative predictive value.

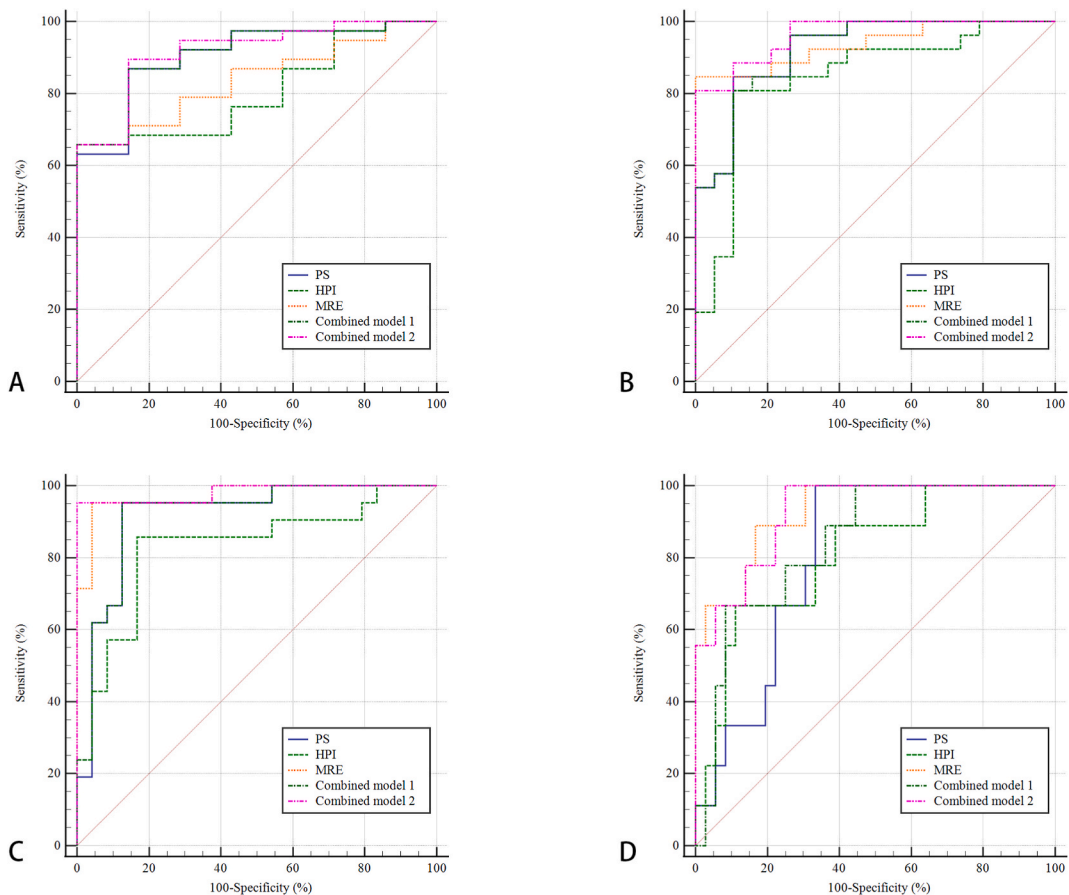


Fig. 6. Receiver operating characteristic curves of liver elastance values and multiphase dynamic enhanced PS parameters for detecting liver fibrosis, F1-4 (A); significant fibrosis, F2-4 (B); progressive fibrosis, F3-4 (C); and cirrhosis, F4 (D).

parameters (PS and HPI) in the exchange model were slightly greater than those of MRE-LSM in diagnosing the presence or absence of liver fibrosis. There was an increase in AUC in combined model 2 compared to MRE-LSM for the diagnosis of fibrosis \geq F1, F2, and F3. There was no significant difference among the MRE, DCE-MRI, and combined models in the diagnosis of any fibrosis stage. The MRE technique was faster to perform than the DCE-MRI technique (shorter scanning and postprocessing times).

In this study, as the severity of liver fibrosis increased, HPI increased; Fp, PS, and Vp decreased; and Fp, PS, and HPI had good diagnostic value for the differential diagnosis of NAFLD liver fibrosis stages. Pathologically, liver fibrosis is an accumulation of extracellular matrix components in the liver, and steatohepatitis in NAFLD patients promotes the activation of hepatic stellate cells (HSCs) [33]. The production of large fibrous collagen molecules deposited in the extravascular space leads to the formation of a basement membrane for hepatic sinusoidal cells and the capillarization of these cells [34]. Liver fibrosis will therefore impede the exchange of vascular and histological interstitial material, while a large amount of extracellular matrix will be deposited in the extravascular space, causing increased resistance to blood flow in the hepatic sinusoids and consequently decreased perfusion in the liver. Hagiwara et al. [35] showed that with the exacerbation of liver fibrosis, the Fp gradually decreased, and the velocity of this flow decreased. Therefore, both PS and Fp should decrease with the exacerbation of liver fibrosis.

In this study, the PS and Fp parameters decreased as the stage of liver fibrosis increased, thus supporting the theoretical hypothesis. Wu et al. [36] performed a quantitative study using a rat liver fibrosis model and found that Ktrans (Ktrans in the extended Tofts model is equivalent to PS and Fp in the exchange model) increased as the fibrosis stage increased. Wu et al. [36] believe that the reason for the increase in Ktrans is that Gd-EOB-DTPA is a small molecule contrast agent that is not affected by the deposition of an extracellular matrix (ECM). Wu et al. [36] suggested that as the stage of liver fibrosis progresses, the increase in the hepatic artery blood supply fraction will increase the transport speed of the contrast agent. The researchers in the present study suggest that the increase in Ktrans in the study by Wu et al. [36] may be due to the use of the contrast agent Gd-EOB-DTPA, which is taken up by hepatocytes and therefore requires an increase in the calculated size of the third compartment of the intracellular space in terms of pharmacokinetics, whereas the study by Wu Z used a two-input extended Tofts model, which is only a two-compartment model and ignores the effect of the third compartment of the contrast agent taken up by hepatocytes in the calculation of quantitative parameters. Despite the use of Gd-EOB-DTPA contrast in the studies of Zou et al. [26] and Liu et al. [27], the Ktrans parameter of DCE-MRI in their studies still had high diagnostic efficacy in diagnosing the early stages of liver fibrosis. In another study, Li et al. [29] used the contrast agent Gd-DTPA-BMA in a rabbit liver fibrosis model. They found that Ktrans values decreased with increasing liver fibrosis, and their results were consistent with this study.

Capillarization of the hepatic sinusoids and deposition of collagen fibers in the tissue interstices results in increased resistance to blood flow in and out of the hepatic sinusoids, decreased hepatic perfusion, and impaired blood microcirculation to hepatocytes. In advanced liver fibrosis, further destruction of liver lobules and formation of pseudolobules increase the intrahepatic vascular pressure, which further increases the vascular resistance of the portal venous system. The corresponding decrease in hepatic blood flow leads to a compensatory response of hepatic artery dilation and subsequent elevation of the hepatic artery fraction to maintain total blood flow to the liver, thus causing an increase in the hepatic artery fraction [37]. The HPI also showed a good correlation with the liver fibrosis stage in this study. HPI values increased as the fibrosis stage increased, and Fp values decreased as the fibrosis stage increased, which is consistent with the pathological change process of liver fibrosis. The HPI can reflect the degree of hepatic vascular arterialization; therefore, the HPI has clinical value in assessing the stage of liver fibrosis.

The parameters Kep and Ve did not correlate statistically with the pathological stage of liver fibrosis, while Vp was negatively associated with liver fibrosis. The Kep and Vp parameter values in the present study were consistent with the findings of Li et al. [29]. Ve was not correlated with liver fibrosis in the present study but was negatively correlated with fibrosis in the study by Li et al. [29]. Theoretically, ECM deposition in the interstitium increases with the progression of fibrosis. Li et al. [29] explained the reason for the reduced Ve as the proliferation of fibrosis-related cells. The reason for the discrepancy between our study and Li's conclusion may be that the rat CCl₄ model used in their research is less prone to steatosis. In contrast, almost all the NAFLD patients in the present study had hepatocellular steatosis, which would cause reduced extravascular extracellular space (EES). Therefore, two factors influenced the Ve parameters, resulting in a nonsignificant Ve parameter. There are fewer studies on Kep, Ve, and Vp; most studies focus more on Ktrans. The present study initially explores these relevant parameters, but more cases are needed to validate them.

MRE has been shown to correlate well with liver fibrosis and has been used as an essential reference standard in liver disease guidelines. In previous studies, MRE was somewhat deficient in its ability to identify early fibrosis [15,38]. First, the MRE-LSM of the liver in normal, healthy individuals is an interval range value [39]. Second, the degree of mechanical alteration of the liver in early fibrosis in NAFLD is small. Therefore, MRE is slightly less accurate in diagnosing early fibrosis than advanced liver fibrosis. In addition, liver MRE-LSM are affected by blood perfusion. Furthermore, the patients included in this study were all NAFLD patients; thus, the diagnostic efficacy in identifying liver fibrosis above stage F1 was reduced and may have been influenced by steatosis and inflammation. Nevertheless, MRE is the most effective imaging tool for detecting liver fibrosis. Indeed, this study confirms that MRE is still an excellent diagnostic tool for identifying all stages of fibrosis.

DCE-MRI can be used to evaluate liver fibrosis by MRE directly evaluates liver stiffness through changes in mechanical waves. The effect of early fibrosis on peripheral perfusion/microcirculation may be greater than that of overall liver stiffness, as in advanced liver fibrosis, the ECM has deposited a large amount of collagen fibers into the extracellular space, leading to changes in blood perfusion. Advanced fibrosis is associated with smaller changes in blood perfusion than early fibrosis, and imaging may also reveal perfusion related to portal hypertension in advanced fibrosis. At this point, the deposition of collagen fibers and portal hypertension will increase the stiffness of the liver. This may explain the current findings that in early fibrosis, the AUC of DCE-MRI was slightly higher than that of MRE, while in advanced fibrosis, the AUC of DCE-MRI was lower than that of MRE.

Imajo K et al. [40] reported that the ICC of interobserver repeatability between an expert and trainee increased with the number of

cases that the trainee had experienced. Regarding operation, DCE-MRI is more cumbersome than MRE, and operators greater experience to become familiar with the operation. In this study, the scanning and postprocessing times of MRE and DCE-MRI were compared; MRE measurements were easier, postprocessing times were shorter, and the technique was easier to implement in clinical applications.

The present study has some shortcomings, such as a small sample size. Additionally, because the temporal resolution of DCE-MRI is low, the diagnostic efficacy of the parameters may be reduced. Additionally, in this study, because of the different technical principles of DCE-MRI and MRE, two ROI drawing methods were used. In DCE-MRI, three ROIs in the right lobe and segment 4 on the largest slice of the liver were selected, and the mean was calculated. Segments 2 and 3 of the liver are easily affected by heartbeat, so measurements are taken in the right lobe and segment 4 of the liver. The principle of DCE-MRI is different from that of MRE. Small blood vessels have little effect on MRE, but they can have a certain impact on DCE measurement. Therefore, DCE-MRI requires more liver segments for measurement. The MRE passive driver is closer to the liver segment 4 region, and for some patients, the MRE-LSM calculation is incorrect in some areas of liver segment 4, which may have led to some differences in the diagnostic efficacy of the two methods. In recent years, NAFLD has been renamed twice, and different naming diagnostic criteria have differences. This study was a retrospective trial, and subjects were enrolled from the clinic according to the NAFLD criteria. Therefore, there may be some bias in patient selection in this study.

5. Conclusion

In conclusion, MRE has good diagnostic value for all stages of liver fibrosis in patients with NAFLD. There was no significant difference in the diagnostic efficacy of DCE-MRI and MRE for any stage of fibrosis in this study. In the absence of MRE equipment, DCE-MRI represents an alternative technique. MRE is a quicker and simpler method of assessing fibrosis than DCE-MRI in the clinic.

Data availability statement

Data will be made available on request.

CRediT authorship contribution statement

Hao Ren: Writing – original draft, Software, Formal analysis, Data curation, Conceptualization. **Dawei Yang:** Writing – review & editing, Formal analysis, Data curation. **Hui Xu:** Software, Resources, Data curation. **Xiaofei Tong:** Resources. **Xinyan Zhao:** Resources, Data curation. **Qianyi Wang:** Resources. **Yameng Sun:** Resources. **Xiaojuan Ou:** Resources. **Jidong Jia:** Resources. **Hong You:** Resources. **Zhanchang Wang:** Resources. **Zhengan Yang:** Writing – review & editing, Software, Resources, Funding acquisition, Formal analysis, Data curation, Conceptualization.

Declaration of competing interest

The authors declare the following financial interests/personal relationships which may be considered as potential competing interests: Zhengan Yang reports financial support was provided by National Natural Science Foundation of China (61871276, 62171298). Zhengan Yang reports financial support was provided by Capital's Funds for Health Improvement and Research (2018-2023). Dawei Yang reports financial support was provided by National Natural Science Foundation of China (82071876, 82372043). Dawei Yang reports financial support was provided by Beijing Natural Science Foundation (7184199). If there are other authors, they declare that they have no known competing financial interests or personal relationships that could have appeared to influence the work reported in this paper.

References

- [1] C. Estes, Q.M. Anstee, M.T. Arias-Loste, et al., Modeling NAFLD disease burden in China, France, Germany, Italy, Japan, Spain, United Kingdom, and United States for the period 2016-2030, *J. Hepatol.* 69 (4) (2018) 896–904.
- [2] F. Zhou, J. Zhou, W. Wang, et al., Unexpected rapid increase in the burden of NAFLD in China from 2008 to 2018: a systematic review and meta-analysis, *Hepatology* 70 (4) (2019) 1119–1133.
- [3] M. Eslam, P.N. Newsome, S.K. Sarin, et al., A new definition for metabolic dysfunction-associated fatty liver disease: an international expert consensus statement, *J. Hepatol.* 73 (1) (2020) 202–209.
- [4] M.E. Rinella, J.V. Lazarus, V. Ratziu, et al., A multisociety Delphi consensus statement on new fatty liver disease nomenclature [published online ahead of print, 2023 Jun 24], *Hepatology* (2023), <https://doi.org/10.1097/HEP.0000000000000520>.
- [5] Y. Yilmaz, The heated debate over NAFLD renaming: an ongoing saga, *Hepatol Forum* 4 (3) (2023) 89–91. Published 2023 Sep. 7.
- [6] M. Ekstedt, H. Hagström, P. Nasr, et al., Fibrosis stage is the strongest predictor for disease-specific mortality in NAFLD after up to 33 years of follow-up, *Hepatology* 61 (5) (2015) 1547–1554.
- [7] P.S. Dulai, S. Singh, J. Patel, et al., Increased risk of mortality by fibrosis stage in nonalcoholic fatty liver disease: systematic review and meta-analysis, *Hepatology* 65 (5) (2017) 1557–1565.
- [8] H. Hagström, P. Nasr, M. Ekstedt, et al., SAF score and mortality in NAFLD after up to 41 years of follow-up, *Scand. J. Gastroenterol.* 52 (1) (2017) 87–91.
- [9] N. Chalasani, Z. Younossi, J.E. Lavine, et al., The diagnosis and management of nonalcoholic fatty liver disease: practice guidance from the American Association for the Study of Liver Diseases, *Hepatology* 67 (1) (2018) 328–357.
- [10] G. Lassailly, R. Caiazzo, D. Buob, et al., Bariatric surgery reduces features of nonalcoholic steatohepatitis in morbidly obese patients, *Gastroenterology* 149 (2) (2015) 379-e16.

- [11] R. Loomba, D.Q. Huang, A.J. Sanyal, et al., Liver stiffness thresholds to predict disease progression and clinical outcomes in bridging fibrosis and cirrhosis, *Gut* 72 (3) (2023) 581–589.
- [12] I.N. Guha, J. Parkes, P. Roderick, et al., Noninvasive markers of fibrosis in nonalcoholic fatty liver disease: validating the European Liver Fibrosis Panel and exploring simple markers, *Hepatology* 47 (2) (2008) 455–460.
- [13] R. Loomba, T. Wolfson, B. Ang, et al., Magnetic resonance elastography predicts advanced fibrosis in patients with nonalcoholic fatty liver disease: a prospective study [published correction appears in *Hepatology*, *Hepatology* 60 (6) (2014) 1920–1928.
- [14] H. Morisaka, U. Motosugi, S. Ichikawa, et al., Magnetic resonance elastography is as accurate as liver biopsy for liver fibrosis staging, *J. Magn. Reson. Imag.* 47 (5) (2018) 1268–1275.
- [15] M. Yin, R.L. Ehman, MR elastography: practical questions, from the AJR special series on imaging of fibrosis [published online ahead of print, 2023 may 10], *AJR Am. J. Roentgenol.* (2023), <https://doi.org/10.2214/AJR.23.29437>.
- [16] D.W. Kim, S.Y. Kim, H.M. Yoon, K.W. Kim, J.H. Byun, Comparison of technical failure of MR elastography for measuring liver stiffness between gradient-recalled echo and spin-echo echo-planar imaging: a systematic review and meta-analysis, *J. Magn. Reson. Imag.* 51 (4) (2020) 1086–1102.
- [17] S. Baxter, Z.J. Wang, B.N. Joe, A. Qayyum, B. Taouli, B.M. Yeh, Timing bolus dynamic contrast-enhanced (DCE) MRI assessment of hepatic perfusion: initial experience, *J. Magn. Reson. Imag.* 29 (6) (2009) 1317–1322.
- [18] M. Oostendorp, M.J. Post, W.H. Backes, Vessel growth and function: depiction with contrast-enhanced MR imaging, *Radiology* 251 (2) (2009) 317–335.
- [19] E. Mormone, J. George, N. Nieto, Molecular pathogenesis of hepatic fibrosis and current therapeutic approaches, *Chem. Biol. Interact.* 193 (3) (2011) 225, 23.
- [20] P.S. Tofts, Modeling tracer kinetics in dynamic Gd-DTPA MR imaging, *J. Magn. Reson. Imag.* 7 (1) (1997) 91–101.
- [21] K. Murase, Efficient method for calculating kinetic parameters using T1-weighted dynamic contrast-enhanced magnetic resonance imaging, *Magn. Reson. Med.* 51 (4) (2004) 858–862.
- [22] T.S. Koh, S. Bisdas, D.M. Koh, C.H. Thng, Fundamentals of tracer kinetics for dynamic contrast-enhanced MRI, *J. Magn. Reson. Imag.* 34 (6) (2011) 1262–1276.
- [23] S. Keller, J. Sedlacik, T. Schuler, et al., Prospective comparison of diffusion-weighted MRI and dynamic Gd-EOB-DTPA-enhanced MRI for detection and staging of hepatic fibrosis in primary sclerosing cholangitis, *Eur. Radiol.* 29 (2) (2019) 818–828.
- [24] K. Juluru, A.H. Talal, R.K. Yantiss, et al., Diagnostic accuracy of intracellular uptake rates calculated using dynamic Gd-EOB-DTPA-enhanced MRI for hepatic fibrosis stage, *J. Magn. Reson. Imag.* 45 (4) (2017) 1177–1185.
- [25] R. Hako, P. Kristian, P. Jarčuška, et al., Noninvasive assessment of liver fibrosis in patients with chronic hepatitis B or C by contrast-enhanced magnetic resonance imaging, *Chin. J. Gastroenterol. Hepatol.* 2019 (2019) 3024630.
- [26] L. Zou, J. Jiang, H. Zhang, et al., Comparing and combining MRE, T1 ρ , SWI, IVIM, and DCE-MRI for the staging of liver fibrosis in rabbits: assessment of a predictive model based on multiparametric MRI, *Magn. Reson. Med.* 87 (5) (2022) 2424–2435.
- [27] H.F. Liu, Q. Wang, Y.N. Du, et al., Dynamic contrast-enhanced MRI with Gd-EOB-DTPA for the quantitative assessment of early-stage liver fibrosis induced by carbon tetrachloride in rabbits, *Magn. Reson. Imaging* 70 (2020) 57–63.
- [28] Z. Wu, Z.L. Cheng, Z.L. Yi, et al., Assessment of nonalcoholic fatty liver disease in rats using quantitative dynamic contrast-enhanced MRI, *J. Magn. Reson. Imag.* 45 (5) (2017) 1485–1493.
- [29] Z. Li, J. Sun, L. Chen, et al., Assessment of liver fibrosis using pharmacokinetic parameters of dynamic contrast-enhanced magnetic resonance imaging, *J. Magn. Reson. Imag.* 44 (1) (2016) 98–104.
- [30] S.P. Sourbron, D.L. Buckley, Tracer kinetic modelling in MRI: estimating perfusion and capillary permeability, *Phys. Med. Biol.* 57 (2) (2012) R1–R33.
- [31] S.B. Donaldson, C.M. West, S.E. Davidson, et al., A comparison of tracer kinetic models for T1-weighted dynamic contrast-enhanced MRI: application in carcinoma of the cervix [published correction appears in *Magn Reson Med.* 2014 Sep;72(3):902], *Magn. Reson. Med.* 63 (3) (2010) 691–700.
- [32] Y.H. Chan, Biostatistics 104: correlational analysis, *Singap. Med. J.* 44 (12) (2003) 614–619.
- [33] R. Bataller, D.A. Brenner, Liver fibrosis [published correction appears in *J Clin Invest.* 2005 Apr;115(4):1100], *J. Clin. Invest.* 115 (2) (2005) 209–218, <https://doi.org/10.1172/JCI24282>.
- [34] V. Hernandez-Gea, S.L. Friedman, Pathogenesis of liver fibrosis, *Annu. Rev. Pathol.* 6 (2011) 425–456, <https://doi.org/10.1146/annurev-pathol-011110-130246>.
- [35] M. Hagiwara, H. Rusinek, V.S. Lee, et al., Advanced liver fibrosis: diagnosis with 3D whole-liver perfusion MR imaging—initial experience, *Radiology* 246 (3) (2008) 926–934, <https://doi.org/10.1148/radiol.2463070077>.
- [36] Z. Wu, Z.L. Cheng, Z.L. Yi, et al., Assessment of nonalcoholic fatty liver disease in rats using quantitative dynamic contrast-enhanced MRI, *J. Magn. Reson. Imag.* 45 (5) (2017) 1485–1493, <https://doi.org/10.1002/jmri.25455>.
- [37] V. Gülberg, K. Haag, M. Rössle, A.L. Gerbes, Hepatic arterial buffer response in patients with advanced cirrhosis, *Hepatology* 35 (3) (2002) 630–634, <https://doi.org/10.1053/jhep.2002.31722>.
- [38] L. Huwart, C. Sempoux, E. Vicaut, et al., Magnetic resonance elastography for the noninvasive staging of liver fibrosis, *Gastroenterology* 135 (1) (2008) 32–40, <https://doi.org/10.1053/j.gastro.2008.03.076>.
- [39] K.M. Pepin, C.L. Welle, F.F. Guglielmo, J.R. Dillman, S.K. Venkatesh, Magnetic resonance elastography of the liver: everything you need to know to get started, *Abdom Radiol (NY)* 47 (1) (2022) 94–114.
- [40] K. Imajo, Y. Honda, T. Kobayashi, et al., Direct comparison of US and MR elastography for staging liver fibrosis in patients with nonalcoholic fatty liver disease, *Clin. Gastroenterol. Hepatol.* 20 (4) (2022) 908–917.e11.